analytical chemistry

Article

pubs.acs.org/ac

$Ru(bpy)_3^{2+}$ Incorporated Luminescent Polymer Dots: Double-Enhanced Electrochemiluminescence for Detection of Single-Nucleotide Polymorphism

Yaqiang Feng, Feng Sun, Ningning Wang, Jianping Lei, and Huangxian Ju*

State Key Laboratory of Analytical Chemistry for Life Science, School of Chemistry and Chemical Engineering, Nanjing University, Nanjing 210023, P. R. China

Supporting Information

ABSTRACT: Encapsulating a large amount of electrochemiluminescence (ECL) active molecules into one nanoparticle for single-target recognition can greatly improve the sensitivity of the ECL assay. This work used luminescent conjugated polymer as a carrier to synthesize $Ru(bpy)_3^{2+}$-doped polymer dots (RuPdots). The RuPdots with an average size of 20 nm and encapsulation of about 1354 $Ru(bpy)_3^{2+}$ showed greatly enhanced ECL emission. Using tripropylamine as a coreactant, the resonance energy transfer from the excited polymer dots to the encapsulated $Ru(bpy)_3^{2+}$ was demonstrated, which led to a 15.7-fold higher ECL emission than that of $Ru(bpy)_3^{2+}$ with the same amount at the gold electrode. By coupling the double-enhanced ECL signal of this nanostructure with the specific ligase detection reaction, a sensitive ECL biosensor was constructed for specific detection of a single-nucleotide polymorphism (SNP). Using mutant *KRAS* gene as a model target, the ECL SNP detection method showed a linear range from 1 fM to 1 nM and a detection limit of 0.8 fM. The designed RuPdots provided a novel signal amplification strategy and could be used as a universal label for ultrasensitive ECL biodetection.

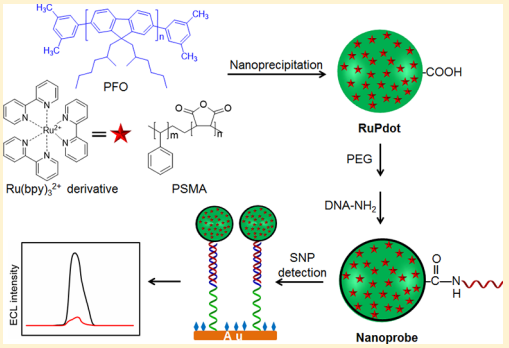

Electrochemiluminescence (ECL) as an analytical technique features electrochemical controllability and low background, and has been widely used in the field of bioanalysis.[1−5] Among various ECL analytical systems, $Ru(bpy)_3^{2+}$ is the most extensively studied luminophore and has been successfully commercialized due to its high ECL efficiency and good stability in aqueous media. Since the discovery of ECL emission of $Ru(bpy)_3^{2+}$ with tripropylamine (TPrA) as a coreactant in acetonitrile solution,[6] many efforts have been carried out to assemble a few $Ru(bpy)_3^{2+}$ monomers as an ECL emitter for improving the ECL efficiency.[7−10] For example, a bimetallic ruthenium complex synthesized by bridging isolated chromophores with bphb (1,4-bis(4′-methyl-2,2′-bipyridin-4-yl)-benzene) showed the ECL emission about 2−3 times stronger than that of $Ru(bpy)_3^{2+}$ in aqueous media,[7] and a supramolecular assembly synthesized by covalently linking eight $Ru(bpy)_3^{2+}$ to the periphery of a carbosilane dendrimer showed the ECL intensity 5 times higher than that of the reference monomeric species.[8] Subsequently, polystyrene microspheres,[9,10] liposomes,[11] and silicon nanoparticles[12,13] have been used as the carriers of a large of $Ru(bpy)_3^{2+}$ to develop ultrasensitive detection methodology. Obviously, encapsulating a large amount of ECL active molecules into single emitter for each target recognition can greatly enhance the ECL emission. However, these methods often require complex and cumbersome organic synthesis processes, and the improvement of ECL efficiency by simply increasing the amount of $Ru(bpy)_3^{2+}$ in the ECL emitter is also very limited. Thus, several new mechanisms for enhancing the ECL emission of $Ru(bpy)_3^{2+}$ have been reported by encapsulating catalytic nanoparticles into dendrimer to facilitate the oxidation of TPrA,[14] introducing localized surface plasmon resonance (LSPR) field effect to increase both the excitation rate and the emission factor of $Ru(bpy)_3^{2+}$,[15,16] and designing intramolecular electron transfer to produce self-enhanced ECL[17] and energy transfer from CdTe quantum dots to enhance the ECL emission of $Ru(bpy)_3^{2+}$.[18] These mechanisms indicated the importance and prospect to probe new mechanisms for improving the ECL emission of $Ru(bpy)_3^{2+}$.

In recent years, conjugated polymer nanoparticles or polymer dots (Pdots) as a kind of new fluorescent nanomaterials have attracted considerable interest.[19−23] Due to their excellent fluorescence brightness, fast emission rate and excellent photostability, these Pdots have been applied in biosensing,[24−26] in vivo imaging,[27−29] controllable drug and gene delivery,[30,31] and single-particle tracking.[32,33] Moreover, the Pdots can act as a new type of excellent ECL nanoemitters.[34,35] Compared to semiconductor quantum dots (QDs),[36,37] they are nontoxic and can be more easily functionalized. However, the ECL application of Pdots is still hampered by low ECL

Received: May 1, 2017
Accepted: June 22, 2017
Published: June 22, 2017

DOI: 10.1021/acs.analchem.7b01603
Anal. Chem. 2017, 89, 7659−7666

Scheme 1. Schematic Diagrams of (A) Preparation of RuPdots Nanoprobe Using PFO, Hydrophobic $Ru(bpy)_3^{2+}$ Derivative, and PSMA; (B) SNP Detection with Ligase Detection Reaction and Nanoprobe

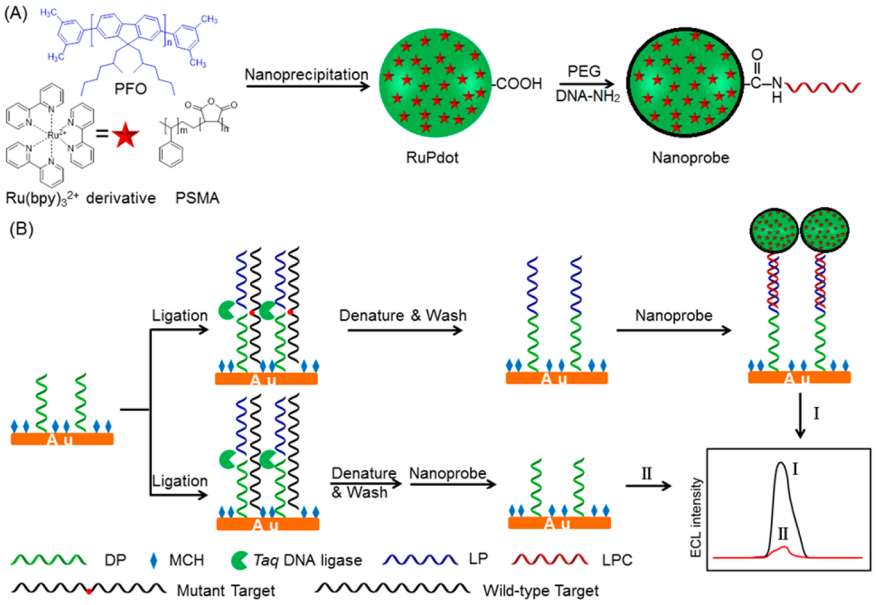

efficiency compared to $Ru(bpy)_3^{2+}$-TPrA system, though the ECL emission of Pdots can be greatly enhanced by regulating the monomer composition[34] and switching the hydrophobicity/hydrophilicity.[35] In order to circumvent this problem, this work integrated the luminescent feature and carrier function of Pdots to design a double-enhanced ECL mechanism by encapsulating a large amount of $Ru(bpy)_3^{2+}$ in Pdots, which could be conveniently synthesized by one-step nanoprecipitation using poly(9,9-dioctylfluorenyl-2,7-diyl) (PFO) as carrier, hydrophobic $Ru(bpy)_3[B(C_6F_5)_4]_2$ as ECL active molecule, and poly(styrene-*co*-maleic anhydride) (PSMA) as functional reagent (Scheme 1A). Compared with other polymers, the PFO not only possessed high fluorescence quantum efficiency but also showed the overlapped fluorescence emission with the absorption of $Ru(bpy)_3^{2+}$. Thus, the high loading of $Ru(bpy)_3^{2+}$ in Pdots as carrier led to multiplex ECL emission for a single-target molecule, and the resonance energy transfer (RET) from excited Pdots to $Ru(bpy)_3^{2+}$ further increased the emission intensity. Thus, the synthesized $Ru(bpy)_3^{2+}$-doped polymer dots (RuPdots) showed excellent ECL properties for sensitive bioanalysis.

Because of the low levels of mutants and excessive amounts of wild-type genes, single-nucleotide polymorphism (SNP) detection with high selectivity and sensitivity is extremely demanding for diseases diagnosis and drug prediction, especially analysis of specific disease-related genetic mutation.[38,39] To meet the sensitivity of SNP detection, PCR and nanomaterials-based signal amplification strategies have been developed for fluorescent detection,[38] light scattering measurement,[40] and surface plasmon resonance imaging,[41] respectively. Here, an ECL method for SNP detection was proposed using DNA-functionalized RuPdots as nanoprobe for signal acquisition and a ligase reaction to endow the method with specificity (Scheme 1B). The analytical performance of the proposed ECL method for detection of mutant *KRAS* gene as a model target demonstrated promising potential of the RuPdots in sensitive biodetection.

EXPERIMENTAL SECTION

Materials and Reagents. PFO (Mw ~ 61 000, polydispersity 3.1) was purchased from American Dye Source, Inc. (Quebec, Canada). Lithium tetrakis (pentafluorophenyl) borate-ethyl ether complex ($Li[B(C_6F_5)_4]_2{\cdot}nEt_2O$) was purchased from TCI (shanghai) Development Co., Ltd. (Shanghai, China). $Ru(bpy)_3Cl_2{\cdot}6H_2O$, PSMA (average Mn ~ 1700), polyethylene glycol (PEG, Mw 3350), 6-mercapto-1-hexanol (MCH), and tris(2-carboxyethyl) phosphine hydrochloride (TCEP) were purchased from Sigma-Aldrich Co., Ltd. (Shanghai, China). *Taq* DNA ligase was obtained from New England Biolabs (Beijing) Ltd. (China). All other reagents were of analytical grade and used as received. 0.1 M phosphate buffer (PB) was prepared by mixing stock solutions of NaH_2PO_4 and Na_2HPO_4. Ultrapure water obtained from a Millipore water purification system (≥18 MΩ, Milli-Q, Millipore) was used in all assays.

All oligonucleotides were synthesized by Shanghai Sangon Biotechnology Co. Ltd. (China). Mutant *KRAS* gene sequence (c.34 G > T) was taken from the database NCBI gene (http://www.ncbi.nlm.nih.gov/gene). All sequences are summarized below:

Discriminating probe (DP): 5′−S-S-$(CH_2)_6$-$(T)_{10}$GCACTCTTGCCTACGCCACA-3′;

Ligation probe (LP): 5′-PO4 AGCTCCAACTACCACAAGTT-3′;

Wild-type *KRAS* gene: 5′-AAACTTGTGGTAGTTGGAGCTGGTGGCGTAGGCAAGAGTGCCTTG-3′;

Mutant *KRAS* gene (c.34 G > T): 5′-AAACTTGTGGTAGTTGGAGCTTGTGGCGTAGGCAAGAGTGCCTTG-3′;

Ligation probe complement (LPC): 5′-NH_2-$(CH_2)_6$-$(T)_{10}$AACTTGTGGTAGTTGGAGCT-3′.

Apparatus. Transmission electron microscopic (TEM) images were acquired on a FEI Tecnai F20 transmission electron microscope (Thermo Fisher Scientific, U.S.A.) with an accelerating voltage of 200 kV for bright field observations, high-angle annular dark field (HAADF) imaging, and energy dispersive X-ray spectroscopic (EDS) analyses. The TEM

DOI: 10.1021/acs.analchem.7b01603
Anal. Chem. 2017, 89, 7659−7666

samples were prepared by directly casting a 10 μg mL^{-1} RuPdots solution onto ultrathin carbon film and followed by drying on desiccator. Dynamic light scattering (DLS) and Zeta potential analysis were performed on a 90 Plus/BI-MAS equipment (Brookhaven, U.S.A.). UV−vis absorption spectra were obtained using a Nanodrop-2000C UV−vis spectrophotometer (Thermo, U.S.A.). Fluorescence measurements were conducted on a F-7000 fluorescence spectrometer (Hitachi Co., Japan) equipped with a xenon lamp. Gel electrophoresis was performed on a Mini-PROTEAN Tetra System and imaged on the Bio-Rad ChemDoc XRS (Bio-Rad, U.S.A.). Electrochemical experiments were performed on a CHI 660B electrochemical workstation (CH Instruments Inc., U.S.A.). ECL measurements were carried out in a self-made cell on a MPI-E multifunctional electrochemical and chemiluminescent analytical system (Xi'an Remex Analytical Instrument Co., Ltd. China).

Synthesis of $Ru(bpy)_3[B(C_6F_5)_4]_2$. Hyrophobic $Ru(bpy)_3[B(C_6F_5)_4]_2$ was synthesized by a metathesis reaction. In brief, $Ru(bpy)_3Cl_2{\cdot}6H_2O$ (74.9 mg, 0.1 mmol) in water was added dropwise to $Li[B(C_6F_5)_4]{\cdot}nEt_2O$ solution (217.2 mg, 0.1 mmol) in water. After the solution was stirred at room temperature for 1 h, the orange-red precipitate was washed by centrifugation (6000 rpm, 20 min) with ultrapure water, and dried at 80 °C for overnight. The precipitate was purified by recrystallization from an acetonitrile/water mixture. The obtained crystalline $Ru(bpy)_3[B(C_6F_5)_4]_2$ was soluble in THF but completely insoluble in water.

Preparation of RuPdots and PFO Pdots. RuPdots was prepared by nanoprecipitation method with slight modification.[34] Initially, 1 mg mL^{-1} stock solutions of PFO, PSMA, and $Ru(bpy)_3[B(C_6F_5)_4]_2$ in THF were first prepared to obtain the mixtures of 10 μg mL^{-1} PFO, 10 μg mL^{-1} PSMA, and $Ru(bpy)_3[B(C_6F_5)_4]_2$ at the relative $Ru(bpy)_3^{2+}$ to PFO weight ratios of 1:1, 2:1, 4:1, respectively. After the mixture was ultrasonically degassed for 20 min under room temperature (Elmasonic P30H, Germany), 2 mL of the mixture was quickly added to 10 mL water in a bath sonicator (120 W, 37 kHz) for 3 min. The solvent THF was then removed by rotary evaporation under vacuum, followed by filtration through a 0.22 μm poly(ether sulfones) (PES) syringe filter (Millex-GP Filter, Millipore). The resulting filtrate was further purified by ultrafiltration (10 kDa, Millipore) centrifugal washing (8000 rpm, 5 min, 4 °C) to remove the free $Ru(bpy)_3[B(C_6F_5)_4]_2$, which was monitored by absorption spectroscopy. The solution of pure RuPdots was yellow and clear. It was stable for months without obvious aggregation.

As control, PFO Pdots were also prepared with a similar method.[34] After the mixture was ultrasonically degassed for 20 min, 2 mL of 10 μg mL^{-1} PFO and PSMA in THF was quickly added to 10 mL of water in a bath sonicator (120 W, 37 kHz) for 3 min, followed with rotary evaporation of THF under vacuum and filtration through PES syringe filter to obtain clear yellow dispersion of PFO Pdots.

Conjugation of RuPdots with DNA. The functionalization of RuPdots with DNA was performed utilizing EDC-catalytic reaction of carboxyl on RuPdots with amine group on DNA.[42,43] PEG (MW 3350) was used for preventing nonspecific adsorption of DNA. In a typical conjugation reaction, 6 μL of HEPES buffer (1 M) and 6 μL of PEG (5% w/v, Mw 3350) were added to 300 μL of RuPdots (2:1) and adjusted the pH to 7.1 with NaOH (0.1 M, ~ 20 μL). After the mixture was mixed homogeneously, 60 μL of ligation probe complement (LCP, 1 μM) and 60 μL of EDC (5 mg mL^{-1}) were added to the mixture and vibrated at room temperature for 2 h. The resulting RuPdot-DNA conjugate was separated by ultrafiltration (10 kDa, Millipore) centrifugal washing (8000 rpm, 3 min, 4 °C) for three times to remove free DNA Finally, the purified RuPdot−DNA conjugate as nanoprobe was diffused in hybridization buffer (10 mM phosphate buffer, 0.25 M NaCl, pH 7.4), and stored in 4 °C for future use.

Immobilization of Discriminating Probe on Gold Electrode. Gold electrodes (3 mm in diameter) were polished on a microcloth with 0.05 μm alumina slurry to a mirror surface, followed by sequential sonication in water, ethanol, and water for 3 min each. Then the electrodes were electrochemically activated in 0.5 M H_2SO_4 solution at 2 V for 5 s and −0.35 V for 10 s, followed by CV scanning from −0.3 to +1.55 V at a scan rate of 4 V s^{-1} for 40 cycles. The activated gold electrodes were thoroughly washed with water and dried under flowing nitrogen.

After the 5′-thiol modified discriminating probe (DP, 100 μM, 5 μL) was activated with TCEP (10 mM, 5 μL) for 1 h to reduce the disulfide, 6 μL of diluted DP (0.1 μM, 10 mM Tris-HCl with 0.1 M NaCl) was immediately dropped on gold electrode and incubated for 2 h at room temperature in 100% humidity. After the electrode was carefully rinsed with 10 mM Tris-HCl (pH 7.4) and dried with nitrogen, it was dipped into 2 mM MCH solution for 2 h at room temperature to block the nonspecific binding sites, rinsed with 10 mM Tris-HCl (pH 7.4) thoroughly, and dried with nitrogen.

SNP Detection. The DP modified electrode was reacted with a mixture of target DNA (mutant *KRAS* gene or wild-type *KRAS* gene at given concentration), ligation probe (LP, 1 nM), and *Taq* DNA ligase (2000 U mL^{-1}) in *Taq* DNA ligase reaction buffer for 2 h at room temperature. After the electrode was washed with 8 M urea solution to denature the protein and then rinsed with hybridization buffer to remove free target, nonligated ligation probe, and *Taq* DNA ligase from electrode surface, the modified electrode was hybridized with nanoprobe for 2 h at room temperature.[38] After it was thoroughly washed with hybridization buffer, the modified gold electrode was used for ECL measurement.

Denaturing Urea-Polyacrylamide Gel Electrophoresis (urea-PAGE). All DNA sequences (DP, LP, mutant *KRAS* gene, and wild-type *KRAS* gene) were annealed at 95 °C for 5 min. Ligation reaction was performed at 65 °C for 30 min in 1 × *Taq* DNA ligase buffer. Samples (5 μL) were in 90% formamide and denatured by boiling for 5 min, followed by rapid cooling in an ice-water bath before loading. Electrophoresis was performed in 20% polyacrylamide gel containing 7 M urea in a 1 × Tris-Borate-EDTA (TBE) buffer with temperature of 65 °C and run at 300 V for 35 min. After the gel was stained with GelRed (Biotium, U.S.A.), it was photographed with a Molecular Imager Gel Doc XR (Bio-Rad, U.S.A.).

Electrochemical and ECL Characterization of RuPdots. The cyclic voltammograms (CVs) were obtained with conventional three-electrode configuration containing the modified gold electrodes (3 mm in diameter) as working electrode, a platinum wire as counter electrode, and an Ag/AgCl electrode (saturated KCl) as the reference electrode. The RuPdots modified gold electrodes were prepared by casting 6 μL of 10 μg mL^{-1} RuPdots solution on an activated gold electrode and dried at room temperature. The ECL curves were obtained by scanning from 0 to +1.2 V in 0.1 M PB containing 0.1 M KNO_3 and 30 mM TPrA (pH 9.0). The ECL window was placed in

DOI: 10.1021/acs.analchem.7b01603
Anal. Chem. 2017, 89, 7659−7666

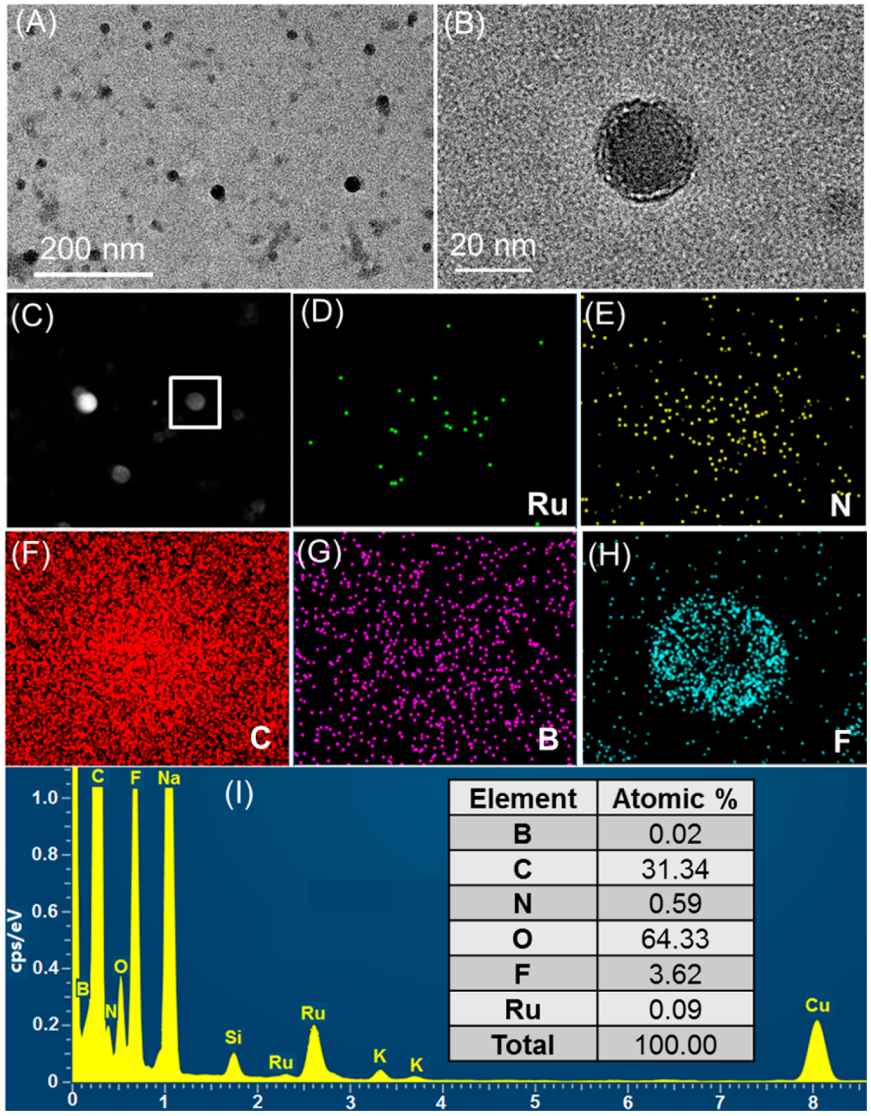

Figure 1. (A) TEM of RuPdots. (B) High-resolution TEM of individual RuPdot. (C) HAADF image with a mapped square region to show the elemental distributions of Ru (D), N (E), C (F), B (G), and F (H). (I) EDS spectrum and atomic percentages of RuPdots.

front of the photomultiplier tube (PMT, detection range: 300−650 nm) biased at −700 V. Unless specifically noted, the scan rate was 100 mV s^{-1}. The ECL spectrum of RuPdots was taken on an inverted fluorescence microscope (Leica DMi8) equipped with an EM-CCD detector (Andor iXon Ultra 897) in conjunction with an electrochemical workstation (CHI 650D) by applying a constant potential of +1.2 V for 2 s.

RESULTS AND DISCUSSION

Characterization of RuPdots. According to the principle of RET, the emission spectrum of the donor must well match the absorption spectrum of the receptor. Thus, the UV−vis absorption and fluorescence emission spectra of $Ru(bpy)_3^{2+}$ and PFO Pdots were first examined. The absorption spectrum of $Ru(bpy)_3^{2+}$ in 400−500 nm showed strong absorption, which completely overlapped with the emission spectrum of PFO Pdots with two peaks at 416 and 443 nm (Figure S1). Moreover, these emission peaks could well separate from that of $Ru(bpy)_3^{2+}$ at 596 nm. These results indicated that PFO Pdots could act as an appropriate candidate of donor to transfer the energy from its excited state to $Ru(bpy)_3^{2+}$ as a receptor. Thus, this work doped $Ru(bpy)_3^{2+}$ in PFO Pdots to design the ECL RET strategy for achieving amplified ECL emission.

Considering the doping efficiency of $Ru(bpy)_3^{2+}$ in PFO Pdots and hydrophobicity of PFO, $Ru(bpy)_3[B(C_6F_5)_4]_2$ was synthesized and dispersed in THF, which showed the UV−vis absorption wavelength and emission peak similar to that of $Ru(bpy)_3^{2+}$ in aqueous solution (Figure S2). Therefore, hydrophobic $Ru(bpy)_3[B(C_6F_5)_4]_2$ was efficiently doped into PFO polymer with nanoprecipitation method (Scheme 1A). The resulting RuPdots showed good solubility in water and the absorption of both $Ru(bpy)_3[B(C_6F_5)_4]_2$ centered at 288 and 450 nm and PFO polymer centered at 370 nm (Figure S3).

To obtain the highly efficient enhancement of ECL emission, the RuPdots with three different doping amounts of $Ru(bpy)_3^{2+}$ was synthesized at 1:1, 2:1, and 4:1 mass concentration ratios of $Ru(bpy)_3^{2+}$ to PFO, respectively. These RuPdots showed the doping amounts of 537, 1354, and 1897 $Ru(bpy)_3^{2+}$ in individual RuPdot (Figure S4, Table S1), respectively. However, the RuPdots obtained at 2:1 showed the highest ECL emission (see below), indicating the best RET efficiency.

DOI: 10.1021/acs.analchem.7b01603
Anal. Chem. 2017, 89, 7659−7666

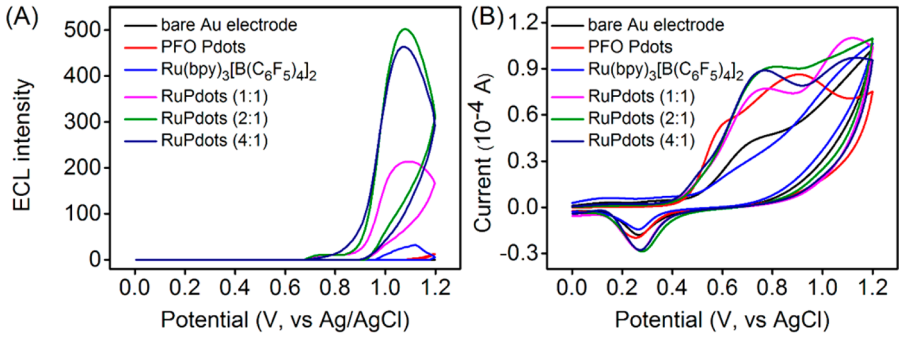

Figure 2. (A) ECL and (B) CV curves of bare and modified Au electrodes with 6 μL of 10 μg mL^{-1} PFO Pdots, 40 μg mL^{-1} $Ru(bpy)_3[B(C_6F_5)_4]_2$, and 10 μg mL^{-1} RuPdots in 0.1 M pH 7.0 PB containing 0.1 M KNO_3 and 30 mM TPrA at 100 mV s^{-1}.

The RuPdots synthesized at the mass concentration ratio of 2:1 was characterized by TEM and EDS mapping. The TEM image revealed an essential spherical morphology and uniform particle size distribution of RuPdots (Figure 1A). The size of RuPdots was about 20 nm (Figure 1B). The incorporation of $Ru(bpy)_3[B(C_6F_5)_4]_2$ in the Pdots was confirmed by TEM coupled with energy-dispersive spectroscopy (TEM-EDS) mapping (Figure 1C−H), which exhibited the distribution of elements Ru, N, C, B, and F, originated from $Ru(bpy)_3[B(C_6F_5)_4]_2$. The TEM−EDS spectrum of RuPdots showed a molar ratio of Ru:N:B:F at 1:6.6:0.2:40.2 (Figure 1I), which was consistent with the theoretical atomic ratio of $Ru(bpy)_3[B(C_6F_5)_4]_2$. These results indicated that hydrophobic $Ru(bpy)_3[B(C_6F_5)_4]_2$ were effectively doped into the Pdots.

Electrochemical and ECL Behaviors of RuPdots. Both the electrochemical and ECL behaviors of different modified electrodes were studied in 0.1 M PB (pH 7.0) containing 0.1 M KNO_3 and 30 mM TPrA as coreactant (Figure 2). Compared with the bare Au electrode, the PFO Pdots modified Au electrode showed a very weak anodic ECL emission at +1.2 V, and the $Ru(bpy)_3[B(C_6F_5)_4]_2$ modified Au electrode displayed a relatively obvious anodic ECL emission at +1.11 V (Figure 2A). The ECL emissions with different intensities and peak positions obviously resulted from different mechanisms. As shown in Figure 2B, TPrA could be oxidized at the bare Au electrode with a peak potential of +0.705 V,[44] which negatively shifted to +0.611 V at the PFO Pdots modified Au electrode due to the good hydrophilicity of PFO Pdots, and almost disappeared at $Ru(bpy)_3[B(C_6F_5)_4]_2$ modified Au electrode due to the hydrophobic electrode surface. Meanwhile, the PFO Pdots modified Au electrode showed another oxidation peak at +0.901 V, which was attributed to the oxidation of PFO Pdots, and thus resulted in a weak ECL emission at +1.2 V due to the reaction of oxidized Pdots ($Pdots^+$) with $TPrA^\bullet$ free radical, a strongly reducing intermediate produced from the electro-oxidation product of TPrA after losing a proton, to produce excited Pdots (Pdots*), as observed in the work reported proviously.[34] The weak ECL emission of $Ru(bpy)_3[B(C_6F_5)_4]_2$ modified Au electrode in TPrA solution followed the general mechanism of $Ru(bpy)_3^{2+}$-TPrA system, at which the oxidation of both TPrA and $Ru(bpy)_3^{2+}$ was hindered by the hydrophobic surface.

Different from above electrodes, all Au electrodes modified with different RuPdots displayed much stronger ECL emission at +1.08 V, while a weak ECL emission was observed at +0.74 V (Figure 2A). Furthermore, these modified electrodes showed both the oxidation peak of TPrA at slightly more positive potentials of +0.761 ∼ + 0.797 V and one oxidation peak at about +1.115 V (Figure 2B). The latter could be attributed to the oxidation of both Pdots and a small amount of encapsulated $Ru(bpy)_3^{2+}$ via hole hopping.[45] Compared to PFO Pdots modified Au electrode, the oxidation peak positively shifted for about 214 mV due to the presence of hydrophobic $[B(C6F5)-4]^-$. Interestingly, with the increase of $Ru(bpy)_3^{2+}$ amount doped in RuPdots, the ECL intensity at +1.08 V increased quickly and then decreased slightly (Figure 2A). The ECL decrease at higher doping amount of $Ru(bpy)_3^{2+}$ was due to the presence of both more hydrophobic $[B(C6F5)4]^-$ and excess ECL active molecules. The former hindered the oxidation of Pdots, and the latter led to the self-quenching phenomenon.[46] Therefore, the RuPdots with the doping ratio of 2:1 was used for this work.

ECL Mechanism of RuPdots Modified Electrode. At RuPdots modified electrodes the oxidation of TPrA at +0.761 ∼ + 0.797 V led to the formation of $TPrA^\bullet$ free radical.[34,44] The free radical could easily be oxidized by $Ru(bpy)_3^{2+}$@Pdots to produce $Ru(bpy)_3^{+}$@Pdots, which was then oxidized by $TPrA^{\bullet+}$, the electro-oxidation product of TPrA, to form $Ru(bpy)_3^{2+}$*@Pdots. Due to the encapsulation of $Ru(bpy)_3^{2+}$ in Pdots, the reaction was hindered by the polymer. Thus, the ECL emission at +0.74 V was very weak and only involved the electro-oxidation of TPrA and the presence of $Ru(bpy)_3^{2+}$@ Pdots on electrode surface (ECL Mechanism I, Supporting Information). In the absence of $Ru(bpy)_3^{2+}$@Pdots, the modified electrodes did not show this emission.

The ECL emission of RuPdots modified electrodes at +1.08 V involved two electro-oxidation processes, Pdots and a small amount of encapsulated $Ru(bpy)_3^{2+}$ at +1.115 V. The oxidation of $Ru(bpy)_3^{2+}$ inside Pdots to produce $Ru(bpy)_3^{3+}$ was limited due to the encapsulation of polymer and the efficient electron tunneling depth of 1−2 nm,[13] and thus, the ECL efficiency from the general way of $Ru(bpy)_3^{2+}$-TPrA system was very low. However, the ECL emission from the Au electrode modified by 2:1 RuPdots showed 15.7 times stronger intensity than that from $Ru(bpy)_3[B(C_6F_5)_4]_2$ modified Au electrode. Obviously, the ECL increase was caused by the oxidation of Pdots to produce $Ru(bpy)_3^{2+}$@$Pdots^+$, which could be quickly reduced by $TPrA^\bullet$ to produce excited $Ru(bpy)_3^{2+}$@Pdots*. Due to the overlap of energy levels of excited Pdots* and $Ru(bpy)_3^{2+}$ (Figures S1 and S2), $Ru(bpy)_3^{2+}$*@Pdots was formed via interior RET (ECL Mechanism II, Supporting Information), which led to an intense emission at 592 nm. It should be pointed out that the formation of $TPrA^\bullet$ involved a deprotonation reaction. Thus, the ECL intensity increases with the increasing pH from 6.0 to 9.0. In addition, the oxidization of polymer to produce soluble product was

DOI: 10.1021/acs.analchem.7b01603
Anal. Chem. 2017, 89, 7659−7666

irreversible,[34] thus the ECL intensity decreased with continuous potential scan.

The ECL RET was further demonstrated with the fluorescence spectrum of $Ru(bpy)_3[B(C_6F_5)_4]_2$ and ECL spectrum of RuPdots modified electrode. The latter showed an ECL emission peak at 592 nm (Figure 3), at which the PFO

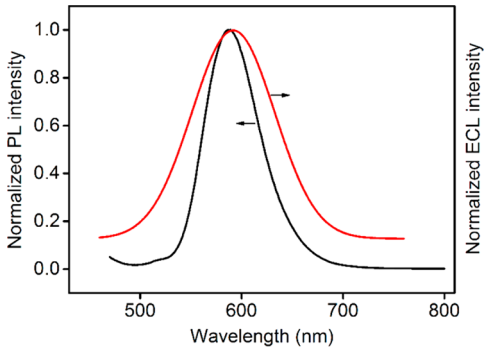

Figure 3. Fluorescence spectrum of 20 μg mL^{-1} Ru(bpy)3[B(C6F5)-4]2 in THF (black) and ECL spectrum of RuPdots modified electrode in 0.1 M pH 7.0 PB containing 0.1 M KNO_3 and 30 mM TPrA at 100 mV s^{-1} (red).

Pdots did not show any emission (Figure S1). On the contrary, $Ru(bpy)_3[B(C_6F_5)_4]_2$ showed the fluorescence emission centered at 587 nm. Thus, the final excited state was $Ru(bpy)_3^{2+*}$. The difference of 5 nm might result from the effect of solvents, as observed in Figures S1 and S2.

Functionalization and Characterization of Nanoprobe. To achieve the biosensing application of the RuPdots with doubly enhanced ECL emission, this work used mutant *KRAS* gene as a target to perform SNP detection. Thus, the RuPdots were functionalized using DNA with LPC sequence through EDC-catalyzed reaction between carboxyl group of RuPdots and amine group of DNA after PEG was adsorbed on the surface for antibiofouling[42,43] (Scheme 1A). The resulting nanoprobe showed an average hydrodynamic diameter of 22.6 nm, slightly larger than that of 20.2 nm for RuPdots (Figure S5A). The similar size distribution profile of the nanoprobe and RuPdots indicated the smooth coating of PEG, which increased the Zeta potential from −6.84 mV to −30.0 mV due to the presence of negatively charged PEG and DNA molecules (Figure S5B).

Detection Principle of SNP Genotyping. According to the previous report,[41] two sequences complementary with two parts of mutation target sequence (T), which were separated by the mutant site, were prepared as DP and ligation probe (LP), respectively. The DP was immobilized on Au electrode surface to capture the target sequence, and the LP could be bound to electrode surface in the presence of the target sequence (Scheme 1B). The LP and DP could be ligated in the presence of *Taq* DNA ligase and the mutant site. On the contrary, no ligation occurred in wild-type target that did not contain the mutant site. Once the ligation reaction was completed, the single-stranded sequence of ligated DP and LP could be formed on the electrode after a stringent washing with urea solution (8 M) for denaturation. The immobilized LP could hybridize with LPC sequence to capture the nanoprobes onto electrode surface for ECL detection. Beyond the mutation target sequence, another wild-type target could not form the ligated DP and LP, and thus, the detection method was specific.

Feasibility of Ligation Reaction. The specificity of ligation reaction was verified by denaturing urea−PAGE gel electrophoresis (Figure 4). After the DP (lane 2, 30 bp) and LP

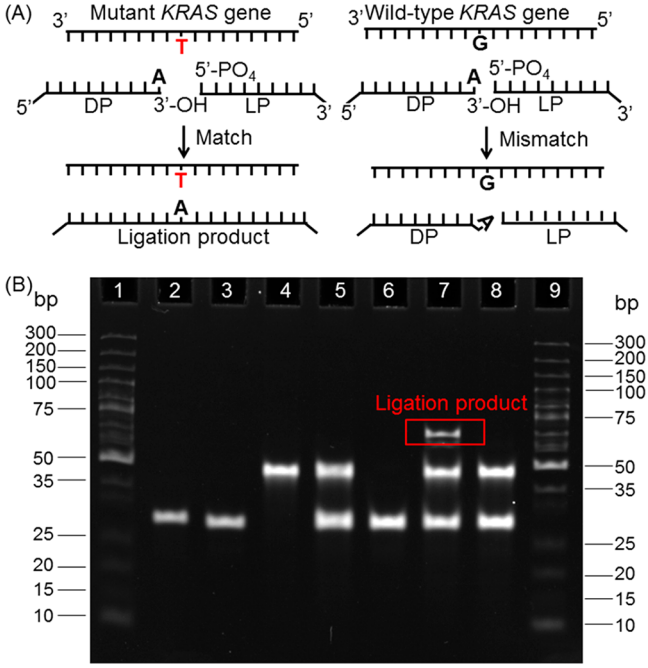

Figure 4. (A) Schematic diagram of the specificity of ligase detection reaction and (B) urea-PAGE of ligation products after denaturation. Lanes 1−9 represent the standard marker (lane 1 and 9), DP (lane 2), LP (lane 3), mutant *KRAS* gene (lane 4), the mixture of DP, LP, and mutant *KRAS* gene (lane 5), the mixture of DP and LP under ligation with *Taq* DNA ligase (lane 6), the mixture of DP, LP, and mutant *KRAS* gene (lane 7) or wild-type *KRAS* gene (lane 8) under ligation with *Taq* DNA ligase.

(lane 3, 30 bp) were hybridized with mutant *KRAS* gene (lane 4, 45 bp) in the presence of *Taq* DNA ligase, a new band was observed at around 60 bp upon thermal and then chemical denaturation (lane 7), confirming the formation of DP-LP ligation product. In the absence of *Taq* DNA ligase or mutant *KRAS* gene, this band did not appear (lanes 5 and 6). Furthermore, in the same conditions wild-type *KRAS* gene did not also produce the new band of ligation product (lane 8), indicating high specificity of the ligation reaction to the mutant site, which provided a specific biosensing strategy for SNP detection.

Analysis of Mutant *KRAS* Gene. *KRAS* mutation can cause abnormal activation of rat sarcoma (*RAS*) proteins to stimulate cell proliferation or differentiation, and ultimately it leads to malignant transformation.[47−49] Moreover, the presence of *KRAS* mutation in nonsmall-cell lung cancer (NSCLC) and metastatic colorectal cancer (mCRC) patients is significantly associated with nonresponse from anti-*EGFR* monoclonal-antibody therapy[50] and has been identified as a key predictor of NSCLC and mCRC. Thus, the detection of *KRAS* mutation has great significance for achieving the maximum therapeutic efficacy in targeted therapy.[51−53] In NSCLC, the *KRAS* mutation usually occurs at codon 12 and 13, which is denoted as G12C, G12 V, and G13D point mutation.[49] This work used G12C point mutation (c.34 G > T) as a target model to demonstrate the specific biosensing strategy by coupling with

DOI: 10.1021/acs.analchem.7b01603
Anal. Chem. 2017, 89, 7659−7666

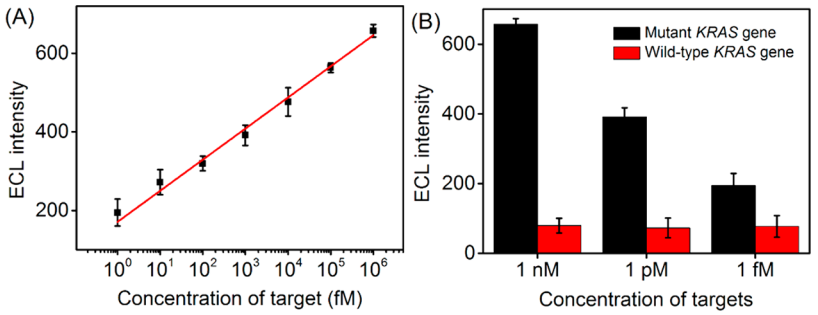

Figure 5. (A) Plot of ECL intensity versus target DNA concentration and (B) ECL intensity for mutant KRAS gene and wily type *KRAS* gene at 1 nM, 1 pM, and 1 fM.

the RuPdots-based ECL nanoprobe for SNP detection (Scheme 1B).

The SNP detection was carried out using a optimum hybridization reaction time of 2 h with a nanoprobe and pH 9.0 (Figure S6). After the nanoprobe was captured to electrode surface by the target-mediated ligation product, the ECL intensity at +1.08 V showed linear increase with the increasing logarithm of mutant *KRAS* gene concentration from 1 fM to 1 nM with a correlation coefficient of 0.997 (Figure 5A). The relative standard deviation (RSD) for five measurements of 1 pM mutant *KRAS* gene was 5.9%, indicating acceptable reproducibility. The limit of detection was 0.8 fM at a signal-to-noise ratio of 3, which was significantly lower than 1 pM of nanoparticle-enhanced surface plasmon resonance imaging,[41] 20 pM of surface-enhanced Raman scattering,[54] and 10 fmol of magnetic beads−ECL system.[55] Moreover, the ECL intensity could be used to clearly distinguish mutant *KRAS* gene and wild-type *KRAS* gene at different concentrations. As shown in Figure 5B, the ECL intensity for mutant *KRAS* gene was 8.3, 5.4, and 2.5 times that for wild-type *KRAS* gene at 1 nM, 1 pM, and 1 fM, respectively. Moreover, other amino acids in detection solution showed little effect on the ECL intensity, except that 8% signal enhancement after addition of 1 μM glycine (Figure S7), demonstrating the high specificity of the proposed ECL SNP detection method.

CONCLUSIONS

This work designs a double-enhanced ECL mechanism by encapsulating a large amount of hydrophobic $Ru(bpy)_3[B(C_6F_5)_4]_2$ in luminescent conjugated polymer with one-step nanoprecipitation. The high loading of $Ru(bpy)_3^{2+}$ in Pdots leads to multiplex ECL emission for a single-target molecule, and the ECL mechanism via RET from excited Pdots to $Ru(bpy)_3^{2+}$ has been demonstrated, which greatly increases the emission intensity. The RuPdots obtained at the doping ratio of 2:1 show the best RET efficiency in the presence of coreactant TPrA. Using mutatnt *KRAS* gene as a target to examine the biosensing application of the RuPdots, the proposed ECL method for SNP detection shows high sensitivity and excellent specificity. This work provides a new ECL and signal amplification strategy, and the designed RuPdots can be used as a universal label for ultrasensitive ECL biodetection.

ASSOCIATED CONTENT

Supporting Information

The Supporting Information is available free of charge on the ACS Publications website at DOI: 10.1021/acs.analchem.7b01603.

UV−vis absorption and fluorescence spectra, doping amount of $Ru(bpy)_3^{2+}$ in RuPdots, estimating the number of $Ru(bpy)_3^{2+}$ in individual RuPdot, ECL mechanism from RuPdots−TPrA system, DLS and zeta potentials of RuPdots and nanoprobe, optimization of detection solution, interference investigation (PDF)

AUTHOR INFORMATION

Corresponding Author

*Phone/Fax: +86-25-89683593. E-mail: hxju@nju.edu.cn.

ORCID

Jianping Lei: 0000-0002-3594-180X

Huangxian Ju: 0000-0002-6741-5302

Notes

The authors declare no competing financial interest.

ACKNOWLEDGMENTS

This work was supported by National Natural Science Foundation of China (21635005, 21361162002), and the program B for outstanding Ph.D. candidate of Nanjing University.

REFERENCES

(1) Bard, A. J. *Electrogenerated Chemiluminescence*; Marcel Dekker: New York, 2004.
(2) Miao, W. *Chem. Rev.* **2008**, *108*, 2506−2553.
(3) Lei, J. P.; Ju, H. X. *TrAC, Trends Anal. Chem.* **2011**, *30*, 1351−1359.
(4) Zhao, W. W.; Wang, J.; Zhu, Y. C.; Xu, J. J.; Chen, H. Y. *Anal. Chem.* **2015**, *87*, 9520−9531.
(5) Liu, Z. F.; Qi, W. J.; Xu, G. B. *Chem. Soc. Rev.* **2015**, *44*, 3117−3142.
(6) Tokel, N. E.; Bard, A. J. *J. Am. Chem. Soc.* **1972**, *94*, 2862−2863.
(7) Richter, M. M.; Bard, A. J.; Kim, W.; Schmehl, R. H. *Anal. Chem.* **1998**, *70*, 310−318.
(8) Zhou, M.; Roovers, J. *Macromolecules* **2001**, *34*, 244−252.
(9) Miao, W.; Bard, A. J. *Anal. Chem.* **2004**, *76*, 5379−5386.
(10) Miao, W.; Bard, A. J. *Anal. Chem.* **2004**, *76*, 7109−7113.
(11) Zhan, W.; Bard, A. J. *Anal. Chem.* **2007**, *79*, 459−463.
(12) Zhang, L.; Dong, S. *Anal. Chem.* **2006**, *78*, 5119−5123.
(13) Zanarini, S.; Rampazzo, E.; Ciana, L. D.; Marcaccio, M.; Marzocchi, E.; Montalti, M.; Paolucci, F.; Prodi, L. *J. Am. Chem. Soc.* **2009**, *131*, 2260−2267.
(14) Kim, Y.; Kim, J. *Anal. Chem.* **2014**, *86*, 1654−1660.
(15) Wang, D.; Guo, L.; Huang, R.; Qiu, B.; Lin, Z.; Chen, G. *Sci. Rep.* **2015**, *5*, 7954.
(16) Wang, D.; Li, Y.; Lin, Z.; Qiu, B.; Guo, L. *Anal. Chem.* **2015**, *87*, 5966−5972.
(17) Wang, H.; Yuan, Y.; Zhuo, Y.; Chai, Y.; Yuan, R. *Anal. Chem.* **2016**, *88*, 2258−2265.

DOI: 10.1021/acs.analchem.7b01603
Anal. Chem. 2017, 89, 7659−7666

(18) Wang, Q.; Chen, M.; Zhang, H.; Wen, W.; Zhang, X.; Wang, S. *Biosens. Bioelectron.* **2016**, *79*, 561−567.
(19) Pecher, J.; Mecking, S. *Chem. Rev.* **2010**, *110*, 6260−6279.
(20) Feng, L.; Zhu, C.; Yuan, H.; Liu, L.; Lv, F.; Wang, S. *Chem. Soc. Rev.* **2013**, *42*, 6620−6633.
(21) Wu, C.; Chiu, D. T. *Angew. Chem., Int. Ed.* **2013**, *52*, 3086−3109.
(22) Peng, H. S.; Chiu, D. T. *Chem. Soc. Rev.* **2015**, *44*, 4699−4722.
(23) Jiang, Y.; McNeill, J. *Chem. Rev.* **2017**, *117*, 838−859.
(24) Ye, F.; Wu, C.; Jin, Y.; Chan, Y.-H.; Zhang, X.; Chiu, D. T. *J. Am. Chem. Soc.* **2011**, *133*, 8146−8149.
(25) Cordovilla, C.; Swager, T. M. *J. Am. Chem. Soc.* **2012**, *134*, 6932−6935.
(26) Li, P.; Liu, L.; Xiao, H.; Zhang, W.; Wang, L.; Tang, B. *J. Am. Chem. Soc.* **2016**, *138*, 2893−2896.
(27) Pu, K.; Shuhendler, A. J.; Jokerst, J. V.; Mei, J.; Gambhir, S. S.; Bao, Z.; Rao, J. *Nat. Nanotechnol.* **2014**, *9*, 233−239.
(28) Palner, M.; Pu, K.; Shao, S.; Rao, J. *Angew. Chem., Int. Ed.* **2015**, *54*, 11477−11480.
(29) Yu, J.; Rong, Y.; Kuo, C. T.; Zhou, X.-H.; Chiu, D. T. *Anal. Chem.* **2017**, *89*, 42−56.
(30) Feng, X.; Lv, F.; Liu, L.; Tang, H.; Xing, C.; Yang, Q.; Wang, S. *ACS Appl. Mater. Interfaces* **2010**, *2*, 2429−2435.
(31) Moon, J. H.; Mendez, E.; Kim, Y.; Kaur, A. *Chem. Commun.* **2011**, *47*, 8370−8372.
(32) Yu, J.; Wu, C.; Sahu, S. P.; Fernando, L. P.; Szymanski, C.; McNeill, J. *J. Am. Chem. Soc.* **2009**, *131*, 18410−18414.
(33) Liu, Z.; Yang, Y.; Sun, Z.; Wu, C. *Opt. Mater.* **2016**, *62*, 1−6.
(34) Feng, Y. Q.; Dai, C. H.; Lei, J. P.; Ju, H. X.; Cheng, Y. X. *Anal. Chem.* **2016**, *88*, 845−850.
(35) Dai, R. P.; Wu, F. M.; Xu, H. F.; Chi, Y. W. *ACS Appl. Mater. Interfaces* **2015**, *7*, 15160−15167.
(36) Gill, R.; Zayats, M.; Willner, I. *Angew. Chem., Int. Ed.* **2008**, *47*, 7602−7625.
(37) Lim, X. *Nature* **2016**, *531*, 26−28.
(38) Syvanen, A.-C. *Nat. Rev. Genet.* **2001**, *2*, 930−942.
(39) Zhong, X.-b.; Reynolds, R.; Kidd, J. R.; Kidd, K. K.; Jenison, R.; Marlar, R. A.; Ward, D. C. *Proc. Natl. Acad. Sci. U. S. A.* **2003**, *100*, 11559−11564.
(40) Bao, Y. P.; Huber, M.; Wei, T.-F.; Marla, S. S.; Storhoff, J. J.; Müller, U. R. *Nucleic Acids Res.* **2005**, *33*, e15.
(41) Li, Y.; Wark, A. W.; Lee, H. J.; Corn, R. M. *Anal. Chem.* **2006**, *78*, 3158−3164.
(42) Wu, C.; Hansen, S. J.; Hou, Q.; Yu, J.; Zeigler, M.; Jin, Y.; Burnham, D. R.; McNeill, J. D.; Olson, J. M.; Chiu, D. T. *Angew. Chem., Int. Ed.* **2011**, *50*, 3430−3434.
(43) Ye, F.; Wu, C.; Jin, Y.; Wang, M.; Chan, Y.-H.; Yu, J.; Sun, W.; Hayden, S.; Chiu, D. T. *Chem. Commun.* **2012**, *48*, 1778−1780.
(44) Li, F.; Zu, Y. *Anal. Chem.* **2004**, *76*, 1768−1772.
(45) Valenti, G.; Rampazzo, E.; Bonacchi, S.; Petrizza, L.; Marcaccio, M.; Montalti, M.; Prodi, L.; Paolucci, F. *J. Am. Chem. Soc.* **2016**, *138*, 15935−15942.
(46) Wang, X.; Wang, Y.; Shan, Y.; Jiang, M.; Li, J. *Int. J. Environ. Anal. Chem.* **2016**, *96*, 1480−1494.
(47) Roock, W. D.; Vriendt, V. D.; Normanno, N.; Ciardiello, F.; Tejpar, S. *Lancet Oncol.* **2011**, *12*, 594−603.
(48) Roberts, P. J.; Stinchcombe, T. E. *J. Clin. Oncol.* **2013**, *31*, 1112−1121.
(49) Karachaliou, N.; Mayo, C.; Costa, C.; Magrí, I.; Gimenez-Capitan, A.; Molina-Vila, M. A.; Rosell, R. *Clin. Lung Cancer* **2013**, *14*, 205−214.
(50) Linardou, H.; Dahabreh, I. J.; Kanaloupiti, D.; Siannis, F.; Bafaloukos, D.; Kosmidis, P.; Papadimitriou, C. A.; Murray, S. *Lancet Oncol.* **2008**, *9*, 962−972.
(51) Thierry, A. R.; Mouliere, F.; El Messaoudi, S.; Mollevi, C.; Lopez-Crapez, E.; Rolet, F.; Gillet, B.; Gongora, C.; Dechelotte, P.; Robert, B.; Del Rio, M.; Lamy, P.-J.; Bibeau, F.; Nouaille, M.; Loriot, V.; Jarrousse, A.-S.; Molina, F.; Mathonnet, M.; Pezet, D.; Ychou, M. *Nat. Med.* **2014**, *20*, 430−435.
(52) Guibert, N.; Ilie, M.; Long, E.; Hofman, V.; Bouhlel, L.; Brest, P.; Mograbi, B.; Marquette, C. H.; Didier, A.; Mazieres, J.; Hofman, P. *Curr. Mol. Med.* **2015**, *15*, 418−432.
(53) Sloane, H. S.; Kelly, K. A.; Landers, J. P. *Anal. Chem.* **2015**, *87*, 10275−10282.
(54) Huh, Y. S.; Lowe, A. J.; Strickland, A. D.; Batt, C. A.; Erickson, D. *J. Am. Chem. Soc.* **2009**, *131*, 2208−2213.
(55) Zhou, H.; Xing, D.; Zhu, D.; Zhou, X. *Talanta* **2009**, *78*, 1253−1258.

DOI: 10.1021/acs.analchem.7b01603
Anal. Chem. 2017, 89, 7659−7666